materials

MDPI

Article

Evaluation and Multi-Objective Optimization of Lightweight Mortars Parameters at Elevated Temperature via Box–Behnken Optimization Approach

Mehmet Kaya [1], Zeynel Baran Yıldırım [2,*], Fuat Köksal [1], Ahmet Beycioğlu [3] and Izabela Kasprzyk [4]

[1] Department of Civil Engineering, Yozgat Bozok University, Yozgat 66100, Turkey; mehmet.kaya@yobu.edu.tr (M.K.); fuat.koksal@yobu.edu.tr (F.K.)
[2] Department of Civil Engineering, Dokuz Eylul University, Izmir 35390, Turkey
[3] Department of Civil Engineering, Adana Alparslan Türkes Science and Technology University, Adana 01250, Turkey; abeycioglu@atu.edu.tr
[4] Faculty of Civil and Environmental Engineering and Architecture, Bydgoszcz University of Science and Technology, 85-796 Bydgoszcz, Poland; izabela.kasprzyk@pbs.edu.pl
* Correspondence: zeynelbaran.yildirim@deu.edu.tr

Abstract: In this research, the mechanical properties of lightweight mortars containing different percentages of additional powder materials has been investigated using response surface methodology (RSM). Box–Behnken design, one of the RSM techniques, was used to study the effects of silica fume content (5, 10, and 15%), vermiculite/cement (V/C) ratio (4, 6, and 8), and temperature (300, 600, and 900 °C) on the ultrasonic pulse velocity (UPV), bending strength, and compressive strength of lightweight mortars. Design expert statistical software was accustomed to determining and evaluating the mix-design of materials in mortar mixtures and temperature effect on mortars. After preliminary experimental research of the relationships between independent and response variables, regression models were built. During the selection of the model parameters, F value, p-value, and R^2 values of the statistical models were taken into account by using the backward elimination technique. The results showed a high correlation between the variables and responses. Multi-objective optimization results showed that the critical temperatures for different levels of silica fume (5–10–15%) were obtained as 371.6 °C, 306.3 °C, and 436 °C, respectively, when the V/C ratio kept constant as 4. According to the results obtained at high desirability levels, it is found that the UPS values varied in the range of 2480–2737 m/s, flexural strength of 3.13–3.81 MPa, and compressive strength of 9.9–11.5 MPa at these critical temperatures. As a result of this research, RSM is highly recommended to evaluate mechanical properties where concrete includes some additional powder materials and was exposed to high temperature.

Keywords: lightweight mortar; silica fume; expanded vermiculite; response surface methodology; box-Behnken design

Citation: Kaya, M.; Yıldırım, Z.B.; Köksal, F.; Beycioğlu, A.; Kasprzyk, I. Evaluation and Multi-Objective Optimization of Lightweight Mortars Parameters at Elevated Temperature via Box–Behnken Optimization Approach. *Materials* **2021**, *14*, 7405. https://doi.org/10.3390/ma14237405

Academic Editor: Gabriele Milani

Received: 1 November 2021
Accepted: 30 November 2021
Published: 2 December 2021

1. Introduction

Due to the scarcity and insufficiency of natural resources, the need for energy has become one of the most important problems of today. In addition, it became difficult to find new energy sources. Therefore, energy efficiency has become an important issue. Energy is consumed in both heating and cooling of buildings. Thermal insulation in buildings is of great importance in terms of energy efficiency. Accordingly, research on new thermal insulation materials are still up-to-date. In addition to thermal insulation in buildings, fire resistance is a situation that should be considered in terms of building safety. Recently, research on the development of cement-based heat-insulating and fire-resistant lightweight composite materials have increasingly continued [1–7].

One of the most important methods known to produce lightweight concrete is to use lightweight aggregate. Another method is to produce concrete with polymer-based

plastic granulated plastic aggregates [8]. Natural or industrial aggregates such as pumice, expanded clay, basalt powder and vermiculite, perlite, blast furnace slag, floor ash are used in concrete production [9–11]. Concretes produced with lightweight aggregates have positive properties such as heat [12–14] and sound insulation [15–18], reduced structure dead load [19–21], and high-temperature resistance [22–24] due to their low density. Lightweight mortars and concretes present some superior properties for structural applications such as fire resistance, thermal insulation, and sound insulation [15,16,25–37]. In addition, light mortars and concretes provide reductions in the cross-sections of the bearing elements and the earthquake loads acting on the structure by reducing the dead load of the structures [19,38,39].

One of the aggregates used in the production of high temperature resistant and lightweight concrete is vermiculite [13,22]. Vermiculite is a magnesium aluminosilicate clay mineral formed by the natural erosion of mica. Mineralogically, vermiculite, which represents a different group alone, is used as a general term covering all mica minarets (phlogopite, biotite, and hydrobiotite) which have industrial expansion properties. Vermiculite can also be described as aqueous magnesium, aluminum, iron silicate [40].

Vermiculite is a natural mineral and member of the Montmorillonite/Smectite Group. It is also placed in Clay and Mica Groups. Vermiculite is generally extremely hydrated biotite or phlogopite. These characteristic minerals later changed to vermiculite by weathering or hydrothermal processes. Vermiculite structures include water inside the interlayer cavities. The dilution properties are controlled via interlayered cations Mg^{2+} and small amounts of Ca^{2+}, Na^{+}, and K^{+}. It influences the cation range and the level of hydration in the charge, intermediate and discharges layer arrays. The hydration status of vermiculite was determined by the quantity of water layers in the intermediate layer cavity. Water and cations among layers decide the thickness of the structural unit [41–43]. Vermiculites are divided into four groups as metamorphic vermiculite [44], macroscopic vermiculite, clay vermiculite [45], and autogenic vermiculite [46]. Vermiculite is crystallized in the monoclinic system and has a uniform slice. It can be green, yellowish coffee, or even black. Its hardness is between 1, 2 and 2.0 according to the Mohs scale and its specific weight is between 2.4 and 2.7. When vermiculite is suddenly subjected to heat-shock at high temperatures, it extends like an accordion. This characteristic expansion is thought to be due to the vapor pressure caused by the sudden evaporation of crystal water in the structure. The reason why thermal expansion has not yet been fully explained is that even samples containing the same total amount of water by weight can expand at different rates. Chemical bonding and the bonding of the water molecules between the leaves to the structure are other important parameters affecting the expansion event. As a result of the expansion, the bulk density of the material decreases by approximately 10 times from 0.8 g/ m^3 to 0.08 g/cm^3. The decrease in bulk density depends on the quality of the vermiculite and the performance of the furnace where the expansion is performed, and an approximate 30-fold expansion can be achieved as a result of heat treatment [47].

Silica fume, an industrial waste, is a very fine-grained powder obtained by the reduction of high-purity quartzite with coal and wood particles in electric arc furnaces used during the production of silicon metal or ferrosilicon alloys. In the upper parts of the furnaces at low temperatures, SiO gas is rapidly oxidized by contact with air and condenses as amorphous SiO2 to form almost all of the silica fume composition [48]. The unit weight of silica fume changes 250 and 300 kg/m^3 [49]. Silica fume is composed of fine particles with a surface area of about 20,000 m^2/kg [50]. It has been observed that compressive strength is increased [51,52], the interface is improved [53], and high-temperature resistance is increased in concretes produced with silica fume additive [21,52].

In recent years, experimental design methods have been extensively used in engineering studies. One of the experimental design methods is RSM which is used for the optimization of engineering problems and/or industrial processes. This methodology is a statistical method to investigate the best relationship between the dependent and independent parameters in experimental design and to determine their optimal use.

When the literature is examined, it is seen that this method has attracted the attention of the researchers especially in recent years and it has started to be used widely. Yıldırım et al. [54] studied to find optimal conditions for the effective waste coal additive on the effects of asphalt concrete utilizing a RSM strategy. Statistical analysis demonstrated that the model attained from the RSM study is appropriate for representing the best solution group model parameters. Miličević, Štirmer, and Bjegović [55], analyzed the effect of recycled aggregate on basic concrete properties (density, porosity e.g.,) by using Central Composite Design (CCD) and BBD. The comparison of values attained from prediction models with the experimental results showed that the BBD is feasible to find for basic properties of concrete including recycled aggregate and the number of experiments could be decreased. Rooholamini, Hassani, and Aliha [56], used CCD for choosing the best model of macro-synthetic fiber on the mechanical properties of roller-compacted concrete pavement (RCCP). The BBD methodology is accustomed to optimizing variables such as pH 3–7, the flow rate of 0.3–0.7 mL/min, and filter depth of 10–20 as well as seeing the effects of the determined parameters on column performance. The pH value has been shown to be the most important factor affecting the performance characteristics of fluorine removal with a fixed-bad column [57]. Adamu, Mohammed, and Liew [58] examined the effects of high-volume fly ash, crumb rubber, and nano-silica on roller-compacted concrete. Compressive, flexural, and splitting tensile strength were defined as response variables, and optimization of mixture proportions were carried out by using BBD design strategy. Analysis results demonstrated that nano-silica increases the performance and mechanical properties of high-volume fly ash samples of roller-compacted concrete with or without addition of crumb rubber. Asadzadeh and Khoshbayan [59] investigated the optimal conditions for foam concrete production including water, cement, and foam volume to obtain minimum density and maximum compressive strength along with the minimum cost. Total of 15 experimental samples were conducted, and the results were settled as response variables in statistical software for analyzing optimization. It was shown that the cost, compressive strength, and dry density response variables could be optimized simultaneously by BBD approach in foam concretes. Performance properties of the additives used in lightweight concretes have been examined by RSM methods and the usability of these techniques has been proven by many studies. Kockal and Ozturan investigated the optimization of the properties of lightweight fly ash aggregates in the production of high strength lightweight concrete using RSM. The effects of temperature, binder content and binder type independent parameters on specific gravity, water absorption, and crushing strength were evaluated and the process was optimized [60]. Using RSM techniques of lightweight mortars, the effect of curing temperatures, binder contents, and curing times on the compressive strength of geopolymer mortar [61], the effects of thermal permeability in different geometries on conduction and convection events [62], cement content, water ratio, and hydrogen peroxide ratios on pressure and the effects on bending strengths [63] were examined in detail in their studies.

The aim of the paper is to assess the effect of silica fume and expanded vermiculite on the behavior of mortars at elevated temperatures and establish a model depending on the test results by using a computer-based experimental program. It is aimed to see the effects of the changes at different levels of the independent variables on the dependent variables through the models created. In addition, multi-objective optimization cases will be evaluated at the desirability levels determined by simultaneous evaluation of dependent and independent variables. The novelty of this study is the evaluation of silica fume and expanded vermiculite mortars with RSM and the determination of critical temperatures in the conditions of multi-objective optimization.

2. Materials and Methods

CEM I 42.5R was used as cement obtained from Yibitaş cement plant, Yozgat, Turkey. Chemical and physical properties of cement are shown in Table 1.

Table 1. Properties and characteristics of CEM I 42.5 Portland cement, expanded vermiculite, and silica fume.

Chemical Composition of CEM I 42.5 R Portland Cement (%)	
MgO	2.75
Si_2O_2	19.12
AI_2O_3	5.63
Fe_2O_3	2.39
Na_2O	-
CaO	63.17
SO_3	2.74
K_2O	1
Insoluble materials	2.33
Loss on ignition	0.49
Physical Composition of CEM I 42.5 R Portland Cement	
Specific gravity (g/cm^3)	3.09
Blaine specific surface area (cm^2/g)	3114
Initial setting time (min)	150
Final setting time (min)	215
Chemical properties and some characteristics of expanded vermiculite	
Color	Gold
Combustibility	Non-combustible
Shape	According to shape granule
Cation exchange capacity	50–150 meg/100 g
Permeability	95%
Water holding capacity	240% (by weight) 28% (by volume)
pH	8.1
Thermal conductivity	0.066–0.063 W/m K
Bulk density	140 kg/m^3
Specific gravity	0.22
Specific heat	0.20–0.26 kcal/kg °C
Sintering temperature	1150–1250 °C
SiO_2	36.90%
AI_2O_3	17.70%
CaO	3.50%
TiO_2	2.20%
MgO	16.40%
K_2O	2.60%
Na_2O	0.20%
Fe_2O_3	11.20%
Loss on ignition	9.20%
Physical and chemical properties of silica fume	
MgO	1.47
AI_2O_3	1.42
CaO	0.8
SO_3	1.34
$SiO_2 + AI_2O_3 + Fe_2O_3$	89.16
SiO_2	85.35
Fe_2O_3	2.39
Loss on ignition	3.4
Moisture (%)	0.19
Bulk density	0.55–0.65 kg/dm^3
Retaining on 45-micron sieve (%)	0.58
Specific gravity	2.23
Surface area (cm^2/g)	8900

The raw vermiculite procured from the Demircilik vermiculite deposit in Yıldızeli, Sivas, Turkey was used. Chemical properties of expanded vermiculite obtained by annealing raw vermiculite at 600 °C for a period of 10 s are given in Table 1. Physical properties of expanded vermiculite are also given in Table 1. Expanded vermiculite used in this research and its SEM image is given in Figure 1.

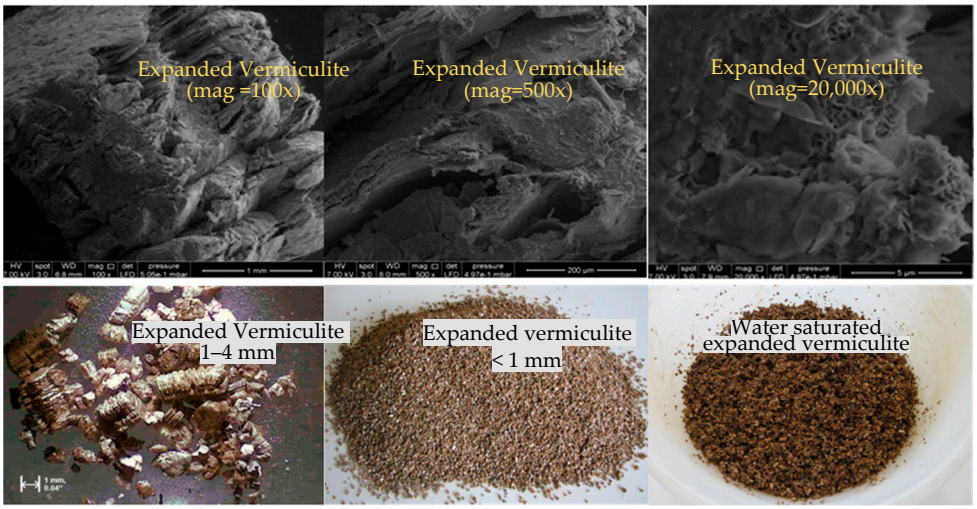

Figure 1. SEM images of expanded vermiculite and the form before use in the mixture.

Besides the expanded vermiculite, in order to obtain higher compressive strength properties on mortars, silica fume additive was provided from Antalya Ferrochrome plants. Silica fume is an amorphous silica with a high specific surface area. The properties of silica fume used in this research are given in Table 1. As seen in Table 1, the total content of SiO_2 + Al_2O_3 + Fe_2O_3 of silica fume is 89.16%. This is an important factor to increase the strength of mortars containing vermiculite. Ultrasound pulse velocities of specimens were determined according to EN 12504-4 standard [64], flexural and compressive tests were also made with respect to EN 1015-11 standard [65].

3. Experimental Design

3.1. Research Objective and Design Process

This study is aimed to investigate some mechanical properties of mortar affected by three inputs parameters. These inputs are silica fume content (5–10–15%), V/C ratio (4–6–8%), and temperature (300, 600, and 900 °C) which were selected as independent variables in experimental design. Within the design process, BBD approach, which is one of the response surface methodologies, was used as experimental design technique. Design Expert 10.0.2 experimental software was employed to generate design strategy, statistical analyses, and the optimization process. The flow chart of the design process shown in Figure 2 was followed step-by-step to select the appropriate design.

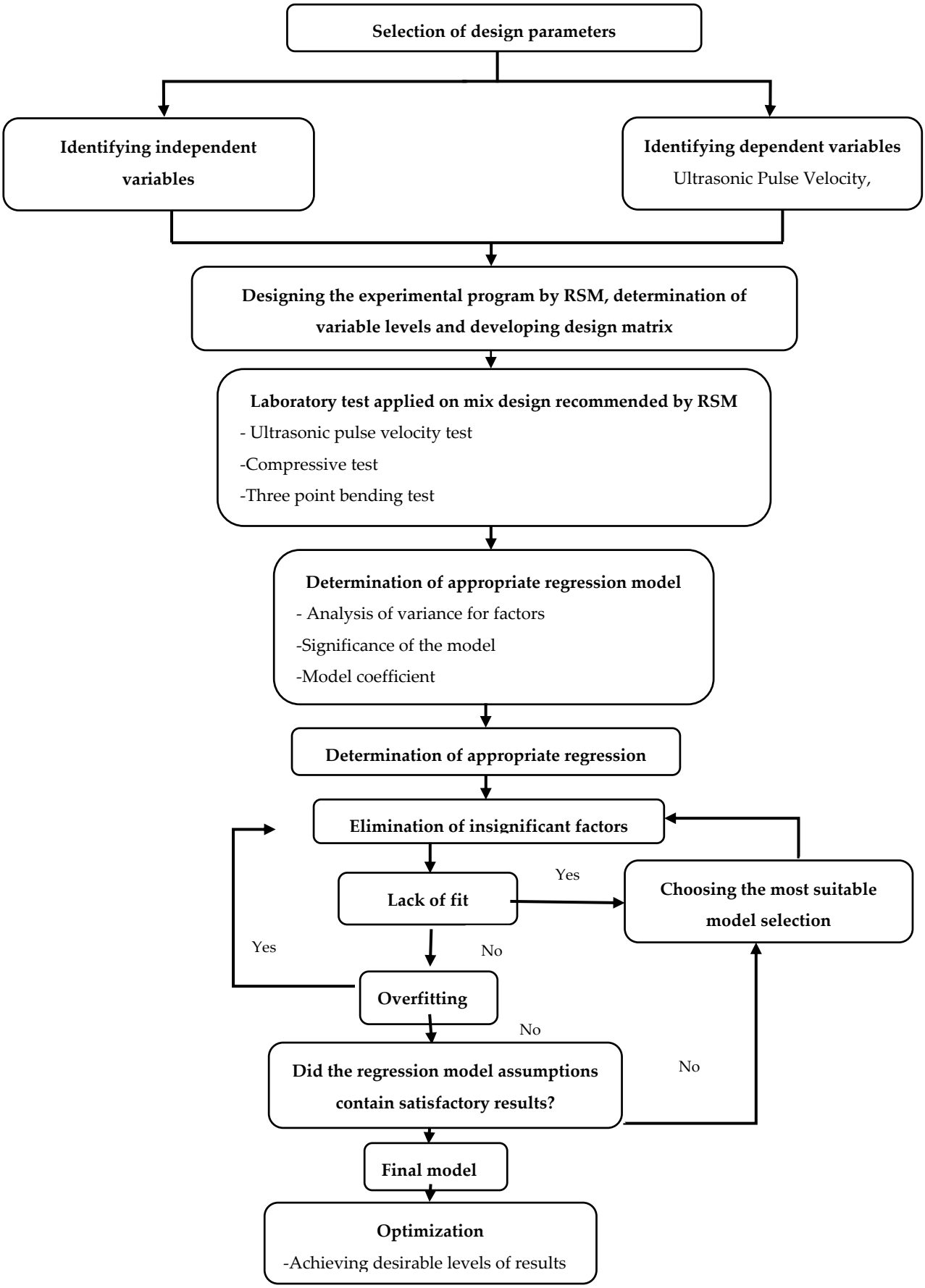

Figure 2. Research process.

3.2. Theory of Experimental Design

RSM is the most appropriate and widely utilized statistical and numerical method used to analyze and develop models of one or more independent parameters that affect a process and the relationships between their responses. Moreover, RSM may be used in the multi-objective optimization model to define desirable targets based on either dependent or independent variables [66,67]. In RSM analysis, there are various design model types according to the suitability of the data used. Among these, the most commonly used methods are CCD and BBD. In RSM applications, there should be appropriate approaches to the interactions between response variables and independent variables. If the response variables are expressed in a linear model in terms of independent variables, the model equation given in Equation (1) is used [68–70].

$$y = \beta_0 + \beta_1 x_1 + \beta_2 x_2 + \ldots + \beta_k x_k + \varepsilon, \quad (1)$$

However, if the curvature effect is significant or the experimental data does not fit to a first-order linear model, the linear model needs to be replaced by a second-order or higher order polynomial model seen in Equation (2).

$$y = \beta_0 + \sum_{i=1}^{n} \beta_i x_i + \sum_{i=1}^{n} \beta_{ii} {x_i}^2 + \sum_{i \neq j=1}^{n} \beta_{ij} x_i x_j + \varepsilon \quad (2)$$

In this equation, y is the modeled response, β is the regression coefficient, i and j are the linear and quadratic coefficient, respectively. x_i and x_j are the coded values of independent variables and the term ε refers to experimental errors [58,66,67,70–72].

In RSM applications, desirability function is widely used to perform optimization of factors and response parameters. Desirability function, one of the popular methods used in simultaneously multi-objective optimization, was first introduced by Harrington [73] and further improved by Derringer and Suich [74]. Maximizing, minimizing, and target functions were utilized while optimizing the independent variables under the desired conditions [66,75,76]. The di values were calculated according to the desirability levels of the response variables. 1 represents the highest degree of desirability while 0 represents the lowest degree of desirability. Mathematical representation of the desirability function is given in Equation (3).

$$D = \left[\prod_{r=1}^{m} d_i \right]^{1/m} \quad (3)$$

3.3. Application of RSM by Using Box–Behnken Design Approach

The factors affecting the mix design are investigated by using BBD. The design is scheduled with the aid of utilizing BBD experimental technique by Design-Expert. Interactions between independent and dependent variables are analyzed by establishing mathematical models. Design matrix consists of 15 experimental series including 3 center points and 12 factorial points. The ranges and levels of the three factors –Silica Fume, V/C, and Temperature–are shown in Table 2.

Table 2. Independent variables and their levels.

		Levels of Code		
Code	Factor	−1	0	+1
A	Silica Fume, %	5	10	15
B	V/C	4	6	8
C	Temperature, °C	300	600	900

In total, 15 experimental runs (3 replicates for the center point, 12 factorial points) in the randomized order were carried out for each response (Silica Fume, V/C, and Temperature). The design matrix generated using coded factors is given in Table 3.

Table 3. Box–Behnken Design for three variables.

Experiment/Mix No.	A	B	C
1	−1	1	0
2	1	1	0
3	0	1	1
4	−1	0	1
5	0	0	0
6	0	1	−1
7	1	−1	0
8	−1	0	−1
9	0	−1	1
10	−1	−1	0
11	0	0	0
12	1	0	−1
13	1	0	1
14	0	−1	−1
15	0	0	0

In the design matrix planned using BBD, variables are defined as follows. The independent variables were Silica fume (x_1), V/C ratio (x_2), and temperature (x_3); and the measured three responses were UPV (y_1), bending strength (y_2), and compressive strength (y_3). The models set for each of the response variables are specified in the following equations.

$$y_1 = \beta_{1,0} + \beta_{1,1}x_1 + \beta_{1,2}x_2 + \beta_{1,3}x_3 + \beta_{1,4}x_1x_2 + \beta_{1,5}x_1x_{3+}\beta_{1,6}x_2x_3 + \beta_{1,7}{x_1}^2 + \beta_{1,8}{x_2}^2 + \beta_{1,9}{x_3}^2 \quad (4)$$

$$y_2 = \beta_{2,0} + \beta_{2,1}x_1 + \beta_{2,2}x_2 + \beta_{2,3}x_3 + \beta_{2,4}x_1x_2 + \beta_{2,5}x_1x_{3+}\beta_{2,6}x_2x_3 + \beta_{2,7}{x_1}^2 + \beta_{2,8}{x_2}^2 + \beta_{2,9}{x_3}^2 \quad (5)$$

$$y_3 = \beta_{3,0} + \beta_{3,1}x_1 + \beta_{3,2}x_2 + \beta_{3,3}x_3 + \beta_{3,4}x_1x_2 + \beta_{3,5}x_1x_{3+}\beta_{3,6}x_2x_3 + \beta_{3,7}{x_1}^2 + \beta_{3,8}{x_2}^2 + \beta_{3,9}{x_3}^2 \quad (6)$$

where $\beta_{1,0}$, $\beta_{2,0}$, $\beta_{3,0}$ are constant; $\beta_{1,1}$, $\beta_{1,2}$, $\beta_{1,3}$, $\beta_{2,1}$, $\beta_{2,2}$, $\beta_{2,3}$, $\beta_{3,1}$, $\beta_{3,2}$, $\beta_{3,3}$ are linear coefficients; $\beta_{1,4}$, $\beta_{1,5}$, $\beta_{1,6}$ $\beta_{2,4}$, $\beta_{2,5}$, $\beta_{2,6}$, $\beta_{3,4}$, $\beta_{3,5}$, $\beta_{3,6}$ are interactive coefficients; $\beta_{1,7}$, $\beta_{1,8}$, $\beta_{1,9}$, $\beta_{2,6}$, $\beta_{2,7}$, $\beta_{2,8}$, $\beta_{2,9}$, $\beta_{3,7}$, $\beta_{3,8}$, $\beta_{3,9}$ are quadratic coefficients.

4. Laboratory Experiments according to Box–Behnken Design

In experimental design conducted by using BBD approach, it was recommended to prepare 15 different mortar mixes for laboratory experiments as seen in Table 3. The mechanical properties of these mortars found experimentally were needed as dependent variables in statistical analysis to find optimum design parameters. Expanded vermiculite aggregates were wetted with half of the water used in the mortar mixture one hour before mixing in the Hobart mixer. While mixing the mortars, vermiculite aggregates wetted after mixing silica fume and cement were added. Then the rest of the water required for the mixture was added.

After mixing all the materials for 3 min, fresh mortar samples were poured into molds of 40 × 40 × 160 mm size. Mortar specimens were kept at room temperature (20 °C) for 24 h. The specimens were then demolded and cured in 23 °C water for 27 days.

After the curing process was completed, the mortar samples were heated at 300, 600, and 900 °C. These temperatures are considered as critical temperatures for the cement paste to start the dehydration process. It is known that in case of fire, high-temperature exposure is only a few hours. For this reason, it is preferred to expose mortar samples to high temperature for 6 h. The temperature in the furnace was adjusted to increase by 5 °C per minute. During the heating of the samples in the furnace, the moisture in its contents are set free. After the heating process is completed, the mortar samples are allowed to cool slowly under 20 °C laboratory conditions. Then, bending and compressive strengths were

determined according to TS EN 12390-5 [77] and TS EN 12390-3 [78] standards and UPV was determined according to ASTM C 597 [79].

5. Results and Discussions

Table 4 shows the BBD and the experimentally obtained responses (i.e., UPV, Bending Strength, and Compressive Strength). The value range from 2181 m/s to 2737 m/s, 0.90 MPa to 3.80 MPa, 3.50 MPa to 11.80 MPa for the UPV, bending strength and compressive strength, respectively.

Table 4. Design matrix and responses obtained.

Run No	Silica Fume (%)	V/C	Temperature °C	UPV (m/s)	Bending Strength (MPa)	Compressive Strength (MPa)
	x_1	x_2	x_3	y_1	y_2	y_3
1	5	8	600	2181	1.8	5.3
2	15	8	600	2173	2.1	6.1
3	10	8	900	2227	0.9	3.5
4	5	6	900	2537	1.2	4.4
5	10	6	600	2380	2.5	7.9
6	10	8	300	2267	2.2	6.2
7	15	4	600	2737	3.0	10.9
8	5	6	300	2305	2.4	7.1
9	10	4	900	2595	1.2	8.1
10	5	4	600	2564	2.9	9.3
11	10	6	600	2385	2.6	7.8
12	15	6	300	2546	2.9	9.9
13	15	6	900	2328	1.0	5.1
14	10	4	300	2594	3.8	11.8
15	10	6	600	2408	2.7	8.0

In experimental design, variance analysis is used to evaluate whether independent parameters have a statistically significant effect on dependent parameters. In the statistical analysis, in addition to independent parameter effects (linear), two-factor interactions and quadratic form of independent parameters on dependent parameters may be observed, if it is appropriate to statistically significant levels [80–82]. In the analysis of variance, the contribution of statistically significant parameters to the model is evaluated by considering the predefined confidence level. In current study, the confidence interval was selected as 95%, which means that the p value was less than 0.05 (p-level < 0.05). In addition, the lack of fit is checked at the significance level of the p-value. If the lack of fit is statistically insignificant and p value of the lack of fit is greater than 0.05, then the model can be evaluated as significant. ANOVA results on response variables are given in Table 5.

The F-values of the models which found as −141.64 for UPV, 177.69 for Bending Strength, and 77.61 for Compressive Strength, demonstrate that the models were all significant, with only 0.09%, 0.01%, and 0.01% possibility, respectively. The significance of all models and terms was controlled using the 95% confidence interval ($p < 0.05$). For UPV, the model and terms B, AB, AC, C^2, A^2B, and AB^2 were significant as their p values were <0.05, whereas A, C, BC, A^2, and B^2 were all insignificant. Bending strength model and its terms A, B, C, AC, BC, A^2, C^2, and A^2 C were all significant as their Prob > F values were <0.05, whereas AB and B^2 were all insignificant. For compressive strength, the model and terms A, B, C, AC, A^2, B^2, and C^2 were all significant as their p values were <0.05, where AB and BC were all insignificant. The empirical models in terms of actual factors for UPV (y_1), bending strength (y_2), and compressive strength (y_3) are presented in Equations (7)–(9).

$$y_1 = 2391 + 8.0 * A - 173.75 * B - 3.12 * C - 45.25 * AB - 112.50 * AC - 10.25 * BC + 15.50 * A^2 + 7.25 * B^2 + 22.50 * C^2 - 63.0 * A^2B + 33.25 * AB^2 \quad (7)$$

$$y_2 = 2.60 - 0.0877 * A - 0.49 * B - 0.98 * C + 0.050 * AB - 0.17 * AC + 0.32 * BC - 0.15 * A^2 - 0.58 * C^2 + 0.20 * A^2C \quad (8)$$

$$y_3 = 7.90 + 0.74 * A - 2.37 * B - 1.74 * C - 0.20 * AB - 0.53 * AC + 0.25 * BC - 0.39 * A^2 + 0.39 * B^2 - 0.89 * C^2 \quad (9)$$

Table 5. ANOVA for developed response models.

Source	Sum of Squares	df	Mean Square	F Value	Prob > F (*p*-Value)
Ultrasonic Pulse Velocity (m/s)					
Model	413,984.6	11	37,635.0	141.64	**0.0009**
A-Silica Fume	256.0	1	256.0	0.96	0.3987
B-V/C	120,756.3	1	120,756.3	454.47	0.0002
C-Temperature	78.1	1	78.1	0.29	0.6253
AB	8190.2	1	8190.2	30.82	0.0115
AC	50,625.0	1	50,625.0	190.53	0.0008
BC	420.3	1	420.3	1.58	0.2975
A^2	887.1	1	887.1	3.34	0.1651
B^2	194.1	1	194.1	0.73	0.4556
C^2	1869.2	1	1869.2	7.03	0.0768
A^2B	7938.0	1	7938.0	29.87	0.0120
AB^2	2211.1	1	2211.1	8.32	0.0633
Residual	797.1250	3	265.7		
Lack of Fit	351.1250	1	351.1	1.57	**0.3363**
Bending Strength (MPa)					
Model	9.9948	10	0.9995	177.69	**0.0001**
A-Silica Fume	0.0612	1	0.0612	10.89	0.0299
B-V/C	1.9013	1	1.9013	338.00	0.0001
C-Temperature	3.8025	1	3.8025	676.00	0.0000
AB	0.0100	1	0.0100	1.78	0.2533
AC	0.1225	1	0.1225	21.78	0.0095
BC	0.4225	1	0.4225	75.11	0.0010
A^2	0.0831	1	0.0831	14.77	0.0184
B^2	0.0000	1	0.0000	0.00	1.0000
C^2	1.2208	1	1.2208	217.03	0.0001
A^2C	0.0800	1	0.0800	14.22	0.0196
Residual	0.0225	4	0.0056		
Lack of Fit	0.0025	2	0.0013	0.13	**0.8889**
Compressive Strength (MPa)					
Model	79.2818	9	8.8091	77.61	**0.0001**
A-Silica Fume	4.3513	1	4.3513	38.34	0.0016
B-V/C	45.1250	1	45.1250	397.58	0.0000
C-Temperature	24.1513	1	24.1513	212.79	0.0000
AB	0.1600	1	0.1600	1.41	0.2884
AC	1.1025	1	1.1025	9.71	0.0264
BC	0.2500	1	0.2500	2.20	0.1979
A^2	0.5544	1	0.5544	4.88	0.0781
B^2	0.5544	1	0.5544	4.88	0.0781
C^2	2.9083	1	2.9083	25.62	0.0039
Residual	0.5675	5	0.1135		
Lack of Fit	0.5475	3	0.1825	18.25	**0.0524**

where A: Silica fume, B: Vermiculite/Cement ratio, C: Temperature, A^2, B^2 and C^2: second order effect, A*B, A*C and B*C two factor interaction effects, A^2B, AB^2 and A^2C qubic effects df: Degree of freedom, F-values: Fisher-statistical test value, *p*-values: Probability values.

The final models' equations were created by removing all insignificant terms for UPV (y_1), bending strength (y_2), and compressive strength (y_3), respectively. These equations are given in Equations (10)–(12).

$$y_1 = 2404.0 - 173.75 * B - 45.25 * AB - 112.50 * AC + 20.87 * C^2 - 63.00 * A^2B + 41.25 * AB^2 \quad (10)$$

$$y_2 = 2.60 + 0.087 * A - 0.49 * B - 0.98 * C - 0.17 * AC + 0.32 * BC - 0.15 * A^2 - 0.58 * C^2 + 0.20 * A^2C \quad (11)$$

$$y_3 = 7.90 - 0.74 * A - 2.37 * B - 1.74 * C - 0.53 * AC - 0.39 * A^2 + 0.39 * B^2 - 0.89 * C^2 \quad (12)$$

After selecting statistically significant parameters for each response variable, the regression model equations of these responses may be obtained. As mentioned in Equations (1)–(3), the interactions can be linear, two factor, and quadratic interactions, the most appropriate statistical model is found and accepted as the regression model of that response variable. The adjusted models for each of the response variables are specified in Equations (4)–(6). The negative and positive signs before a model term indicate the antagonistic or synergistic effects of independent variables on response variables.

The degree of correlation values was used to evaluate the adequacy and quality of the established models. Table 6 shows the coefficients of determination for responses investigated. In Table 6, all of the generated response variable models have significant R^2 values that were greater than 0.85. Thus, nearly 99.38%, 99.68%, and 98.78% of the experimental data of the UPV, bending strength, and compressive strength models, respectively, can be correlated with the models. For the R^2 values of the models to be in good agreement, the difference between the two should be <0.2. As can be seen differences between those values, it is seen that all response variables were in good agreement. In addition, the adequate precision (AP) values are given in Table 6. AP is a parameter that measures the signal to noise ratio, and it has to be greater than 4 to accept the desirability of responses. Considering the AP values, all models were in good agreement. The graphs indicating the relationship between predicted values from the established models and actual values are given in Figure 3a–c for UPV, bending strength, and compressive strength, respectively. As can be seen in Figure 3, the results obtained from the BBD model are very close to the experimental results.

Table 6. Coefficient of determinations for response variables.

Response	R^2	Adj R^2	Pred R^2	A.P.
Ultrasonic Pulse Velocity (m/s)	0.9938	0.9891	0.9094	46.020
Bending strength (Mpa)	0.9968	0.9924	0.9893	51.304
Compressive strength (Mpa)	0.9878	0.9755	0.9287	30.139

where R^2: degree of correlation, Adj R^2: adjusted the degree of correlation, Pred R^2: predicted degree of correlation, A.P: adequate precision.

A three-dimensional (3-D) surface graphs were used to present the relationship between two independent parameters and response parameters. Figure 4a shows 3-D response surface graphs of changes in UPV, the relationship between silica fume and V/C ratio when the temperature is taken as constant 300 °C. Figure 4b shows the relationship between silica fume and temperature, assuming the 3-D response surface graphs of the change in flexural strength, assuming the V/C ratio of 4. Figure 4c shows the 3-D response surface graphs of changes in compressive strength, the relationship between temperature and V/C ratio, when silica fume is taken as constant 10%.

For a better interpretation of the 3D response surface graphs, their 2D cases are also given. The color changes in these graphics represent the 3rd dimension. Blue values indicate low levels of the parameter, red values indicate high levels. Parabolic and linear effects can also be seen on these graphs.

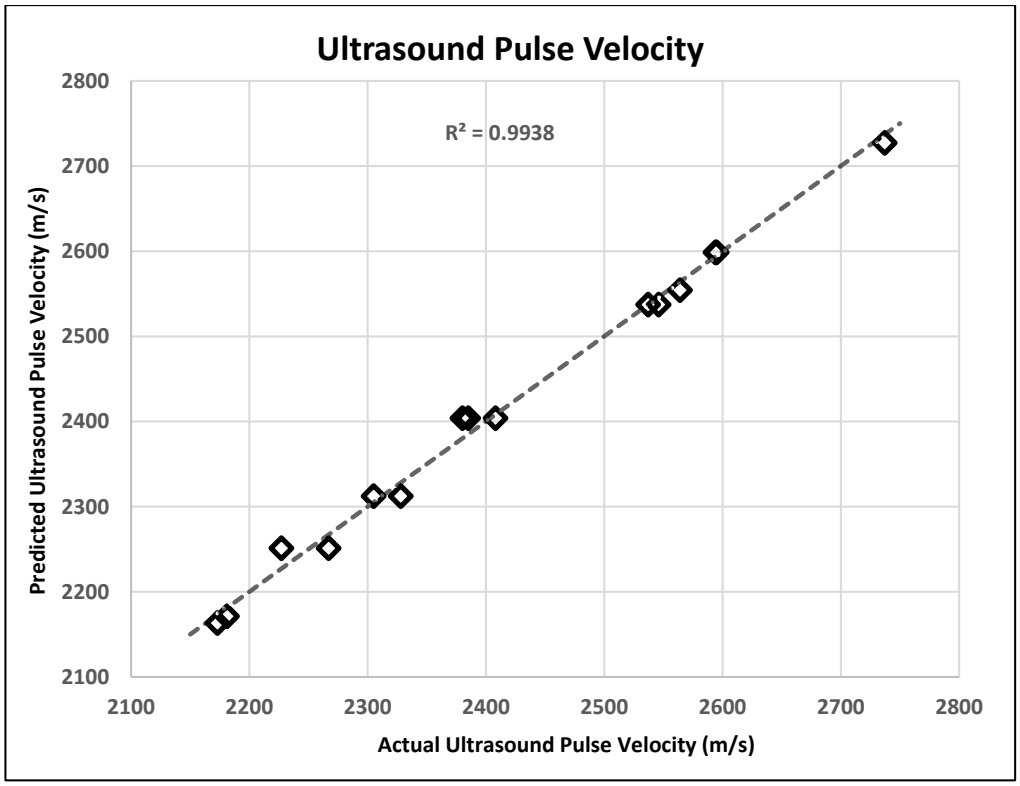

(a)

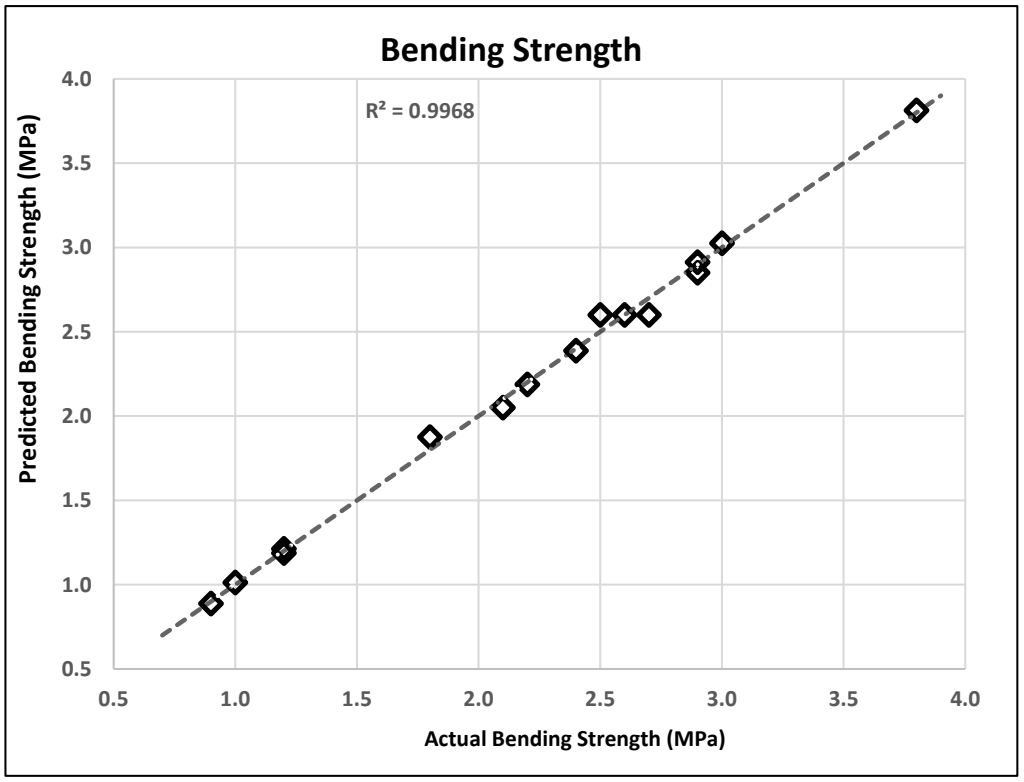

(b)

Figure 3. *Cont*.

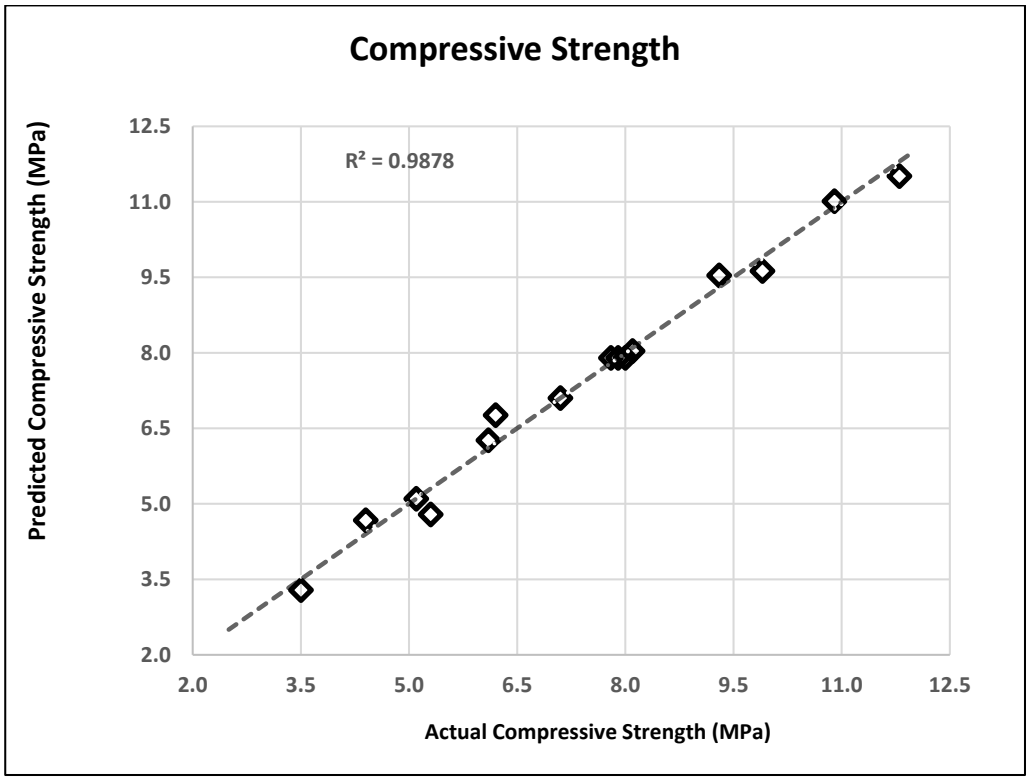

(c)

Figure 3. Relationship between experimental and predicted values of response variable.

When the response surface graphs are analyzed, the interaction between silica fume and V/C (A and B) (Figure 4a) is observed; at low levels of silica fume, the increasing V/C ratio has a parabolic decreasing effect on the UPV value, and at high levels of silica fume, the increase in the V/C ratio has a linear decreasing effect on the UPS value. In addition, increasing silica fume at all levels of the V/C ratio has a slightly increased parabolic effect on the UPS value.

In the interaction between silica fume and temperature (A and C) (Figure 4b), increasing the temperature at all levels of silica fume has a parabolic effect, which initially increases the bending strength value slightly and then decreases it. Moreover, increase in silica fume at all levels of temperature has a parabolic effect, which slightly decreases the bending strength value.

When the interaction between temperature and V/C ratio (B and C) is examined (Figure 4c), an increase in V/C ratio at all levels of temperature exhibits a linear decrease. Moreover, increasing in temperature at all levels of V/C ratio has a parabolic decrease in compressive strength value.

Simultaneously multi-objective optimization is the determination of the proportions of independent variables that can be used to obtain an optimized mortar mix based on the desired performance levels of response variables. In this study, optimization of response parameters was achieved by using desirability function in Design-Expert software version 10.0.2. In the simultaneous optimization criteria, critical temperatures were determined for all combinations of levels of 5–10–15% silica fume and 4–6–8 ratio of V/C. For this purpose, temperature and UPV variables were set to be in range, compressive and bending strength response variables were determined to be at maximum desirable levels as presented in Table 7.

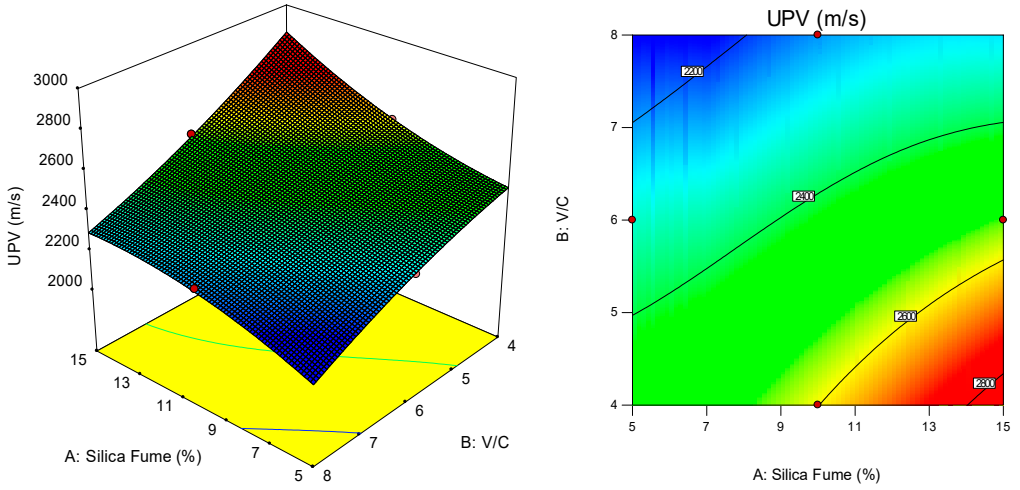

(a)Temperature: 300

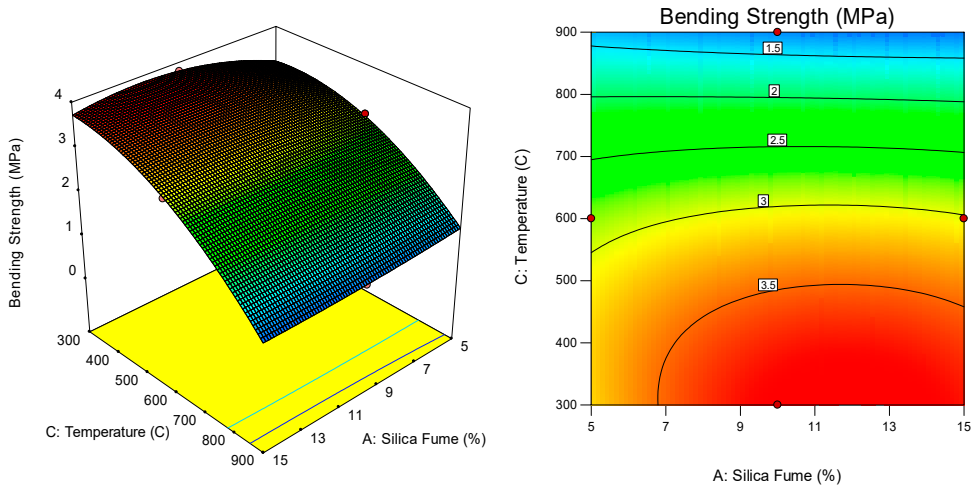

(b)Vermiculite/Cement Ratio: 4

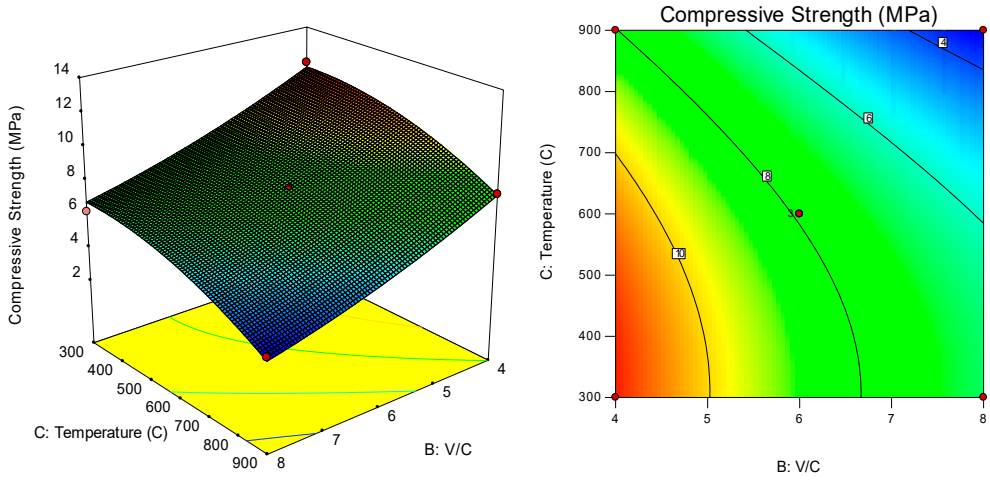

(c) Silica Fume: %10

Figure 4. Influence of independent variables and their interactions on response variables.

Table 7. Multi-objective optimization criteria.

Variables and Responses	Symbol	Goal	Lower Limit	Upper Limit
Silica Fume (%)	A	(%5–10–15)	5	15
V/C	B	(4–6–8)	4	8
Temperature °C	C	In range	300	900
Ultrasonic Pulse Velocity (m/s)	y_1	In range	2173	2737
Bending Strength (MPa)	y_2	Maximize	0.9	3.8
Compressive Strength (MPa)	y_3	Maximize	3.5	11.8

Multi-objective optimization results are presented in Table 8. Desirability is the most important parameter to evaluate the success of optimization. As seen in the table, when the V/C ratio was kept constant as 4 and silica fume levels were chosen as 5%, 10%, and 15%, the critical temperatures were obtained as 371.6 °C, 306.3 °C, and 436 °C with the highest desirability percentages.

Table 8. Optimization with desirability values.

Solution Number	Silica Fume (%)	V/C	Temperature °C	UPV (m/s)	Bending Strength (MPa)	Compressive Strength (MPa)	Desirability (%)
1	5.00	4.00	371.6	2480.7	3.22	9.9	78.9
2	10.00	4.00	306.3	2597.8	3.81	11.5	98.3
3	15.00	4.00	436.605	2737	3.13	11.2	84.4
4	5.00	6.00	423.9	2345.2	2.52	7.2	49.7
5	10.00	6.00	330.2	2420.8	3.01	8.7	67.8
6	15.00	6.00	306.8	2533.9	2.91	9.6	71.6
7	5.00	8.00	604.7	2173	1.87	4.7	22.6
8	10.00	8.00	380.89	2241.4	2.28	6.7	42.9
9	15.00	8.00	364.1	2264.6	2.19	7.5	46.2

6. Conclusions

In this research, the effect of three independent parameters, namely, silica fume, V/C ratio, and temperature on the UPV, bending strength and compressive strength were investigated by using BBD approach. Following conclusions can be written:

- In the design approach, 15 experimental conditions were recommended by BBD. The recommended experimental conditions were applied at the laboratory and the results were found in the range of 2181–2737 m/s, 0.90–3.80 MPa, and 3.50–11.80 MPa for UPV, bending strength, and compressive strength, respectively.
- Statistical models were conducted on the results that were found in the recommended experiments. All models conducted on experimental results were found statistically significant according to p-values, R2 values, AP values, and lack of fit values.
- According to the relationship between dependent and independent variables observed in optimization, UPV value decreases when silica fume increases at high levels of temperature while the increase in silica fume at low levels of temperature exhibits a near-linear increase effect on UPV.
- Increasing temperature at all levels of silica fume has a parabolic effect, which initially increases the bending strength value slightly and then decreases it. Moreover, increasing in silica fume at all levels of temperature has a parabolic effect, which slightly decreases the bending strength value.
- Furthermore, a linear decrease was found in compressive strength when V/C increased. V/C ratio has the same effect on compressive strength at all levels of temperature. A similar decrease in compressive strength was found for an increase in temperature at all levels of V/C ratio.
- An optimization was made to find the maximized mechanical performances of mortar by using statistical models. When the V/C ratio was kept constant as 4 and silica fume levels were chosen as 5%, 10%, and 15%, the critical temperatures were obtained as 371.6 °C, 306.3 °C, and 436 °C with the highest desirability percentages.

As a result of this study, it is seen that the experimental design methods can be very useful for laboratory studies to decrease labor efforts, materials consumption, cost and time period.

Author Contributions: M.K.: investigation, conceptualization, methodology, experimental works, writing;—review and editing; Z.B.Y.: investigation, methodology, experimental works, experimental software, writing; review and editing; F.K.: formal analysis, conceptualization, supervision, methodology, experimental works, writing—review and editing; A.B.: funding acquisition, conceptualization, supervision, formal analysis, writing—review and editing; I.K.: investigation, funding acquisition, formal analysis, writing—review and editing; All authors have read and agreed to the published version of the manuscript.

Funding: The scientific collaborations of this article have been improved by the support of the Polish National Agency for Academic Exchange under Grant No. PPI/APM/2019/1/00003.

Institutional Review Board Statement: Not applicable.

Informed Consent Statement: Not applicable.

Data Availability Statement: Data are summarized in Table 4. They can be requested by contacting the corresponding author.

Conflicts of Interest: The authors declare no conflict of interest in preparing this article.

References

1. Mo, K.H.; Lee, H.J.; Liu, M.Y.J.; Ling, T. Incorporation of expanded vermiculite lightweight aggregate in cement mortar. *Constr. Build. Mater.* **2018**, *179*, 302–306. [CrossRef]
2. Liu, Q.; Liu, W.; Li, Z.; Guo, S.; Sun, G. Ultra-lightweight cement composites with excellent flexural strength, thermal insulation and water resistance achieved by establishing interpenetrating network. *Constr. Build. Mater.* **2020**, *250*, 118923. [CrossRef]
3. Liu, W.V.; Apel, D.B.; Bindiganavile, V. Thermal characterisation of a lightweight mortar containing expanded perlite for underground insulation. *Int. J. Min. Miner. Eng.* **2011**, *3*, 55–71. [CrossRef]
4. Wu, F.; Yu, Q.; Liu, C. Durability of thermal insulating bio-based lightweight concrete: Understanding of heat treatment on bio-aggregates. *Constr. Build. Mater.* **2021**, *269*, 121800. [CrossRef]
5. Lam, T.V.; Vu, D.T.; Dien, V.K.; Bulgakov, B.I.; Korol, E.A. Properties and thermal insulation performance of light-weight concrete. *Mag. Civ. Eng.* **2018**, *84*, 173–191.
6. Akçaözoğlu, K.; Akçaözoğlu, S. The Effect of Elevated Temperature on the Lightweight Concrete Produced by Expanded Clay Aggregate and Calcium Aluminate Cement. *Bilge Int. J. Sci. Technol. Res.* **2017**, *1*, 59–70.
7. Zhu, P.; Brunner, S.; Zhao, S.; Griffa, M.; Leemann, A.; Toropovs, N.; Malekos, A.; Koebel, M.M.; Lura, P. Study of physical properties and microstructure of aerogel-cement mortars for improving the fire safety of high-performance concrete linings in tunnels. *Cem. Concr. Compos.* **2019**, *104*, 103414. [CrossRef]
8. Kan, A.; Demirboğa, R. A novel material for lightweight concrete production. *Cem. Concr. Compos.* **2009**, *31*, 489–495. [CrossRef]
9. Beycioğlu, A.; Başyiğit, C.; Kılınçarslan, Ş.; Şamandar, A. Effect of Mineral admixture on properties of lightweight pumice concrete. *Int. J. Phys. Sci.* **2011**, *6*, 1591–1603.
10. Yoon, J.Y.; Kim, J.H. Mechanical properties of preplaced lightweight aggregates concrete. *Constr. Build. Mater.* **2019**, *216*, 440–449. [CrossRef]
11. Dobiszewska, M.; Schindler, A.K.; Pichór, W. Mechanical properties and interfacial transition zone microstructure of concrete with waste basalt powder addition. *Constr. Build. Mater.* **2018**, *177*, 222–229. [CrossRef]
12. Beycioğlu, A.; Başyişit, C.; Kılınçarslan, Ş. The Effect of Silica Fume on Pumice Aggregate Lightweight Concrete. *J. Nat. Appl. Sci.* **2010**, *14*, 7–11.
13. Köksal, F.; Serrano-López, M.A.; Şahin, M.; Gencel, O.; López-Colina, C. Combined effect of steel fibre and expanded vermiculite on properties of lightweight mortar at elevated temperatures. *Mater. Struct.* **2015**, *48*, 2083–2092. [CrossRef]
14. Alengaram, U.J.; al Muhit, B.A.; Jumaat, M.Z.B.; Jing, M.L.Y. A comparison of the thermal conductivity of oil palm shell foamed concrete with conventional materials. *Mater. Des.* **2013**, *51*, 522–529. [CrossRef]
15. Kim, H.; Lee, H. Influence of cement flow and aggregate type on the mechanical and acoustic characteristics of porous concrete. *Appl. Acoust.* **2010**, *71*, 607–615. [CrossRef]
16. Marlof, A.; Neithalath, N.; Sell, E.; Wegner, K.; Weiss, J.; Olek, J. Influence of aggregate size and gradation on acoustic absorption of enhanced porosity concrete. *ACI Mater. J. Am. Concr. Inst.* **2004**, *101*, 82–91.
17. Tutikian, B.F.; Nunes, M.F.O.; Leal, L.C.; Marquetto, L. Impact sound insulation of lightweight concrete floor with EVA waste. *Build. Acoust.* **2012**, *19*, 75–88. [CrossRef]
18. Tutikian, B.F.; Nunes, M.F.O.; Leal, L.C.; Marquetto, L. Lightweight concrete with EVA recycled aggregate for impact noise attenuation. *Mater. Construcción* **2013**, *63*, 309–316. [CrossRef]

19. Youm, K.S.; Jeong, Y.J.; Han, E.S.H.; Yun, T.S. Experimental investigation on annual changes in mechanical properties of structural concretes with various types of lightweight aggregates. *Constr. Build. Mater.* **2014**, *73*, 442–451. [CrossRef]
20. Swamy, N.V.; Krishnamurthy, M. Seismic performance of lightweight concrete structures. *Adv. Civ. Eng.* **2018**, *2018*, 2105784.
21. Mindess, S. *Developments in the Formulation and Reinforcement of Concrete*; Woodhead Publishing: Sawston, UK, 2019.
22. Koksal, F.; Gencel, O.; Kaya, M. Combined effect of silica fume and expanded vermiculite on properties of lightweight mortars at ambient and elevated temperatures. *Constr. Build. Mater.* **2015**, *88*, 175–187. [CrossRef]
23. Habib, U.; Demirboğa, R.; Şahin, R.; Gül, R. The effects of different cement dosages, slumps, and pumice aggregate ratios on the thermal conductivity and density of concrete. *Cem. Concr. Res.* **2004**, *34*, 845–848.
24. Miloš, J.; Keppert, M.; Výborný, J.; Černý, R. Hygric, thermal and durability properties of autoclaved aerated concrete. *Constr. Build. Mater.* **2013**, *41*, 352–359.
25. Chen, B.; Liu, N. A novel lightweight concrete-fabrication and its thermal and mechanical properties. *Constr. Build. Mater.* **2013**, *44*, 691–698. [CrossRef]
26. Unal, O.; Uygunoglu, T.; Yildiz, A. Investigation of properties of low-strength lightweight concrete for thermal insulation. *Build. Environ.* **2007**, *42*, 584–590. [CrossRef]
27. Demirboga, R.; Gül, R. The effects of expanded perlite aggregate, silica fume and fly ash on the thermal conductivity of lightweight concrete. *Cem. Concr. Res.* **2003**, *33*, 723–727. [CrossRef]
28. Aydın, S.; Baradan, B. Effect of pumice and fly ash incorporation on high temperature resistance of cement based mortars. *Cem. Concr. Res.* **2007**, *37*, 988–995. [CrossRef]
29. Al-Sibahy, A.; Edwards, R. Thermal behaviour of novel lightweight concrete at ambient and elevated temperatures: Experimental, modelling and parametric studies. *Constr. Build. Mater.* **2012**, *31*, 174–187. [CrossRef]
30. Türkmen, I.; Fındık, S.B. Several properties of mineral admixtured lightweight mortars at elevated temperatures. *Fire Mater.* **2013**, *37*, 337–349. [CrossRef]
31. Jin, Z.-F.; Asako, Y.; Yamaguchi, Y.; Harada, M. Fire resistance test for fire protection materials with high water content. *Int. J. Heat Mass Transf.* **2000**, *43*, 4395–4404. [CrossRef]
32. Go, C.-G.; Tang, J.-R.; Chi, J.-H.; Chen, C.-T.; Huang, Y.-L. Fire-resistance property of reinforced lightweight aggregate concrete wall. *Constr. Build. Mater.* **2012**, *30*, 725–733. [CrossRef]
33. Kim, J.-H.J.; Lim, Y.M.; Won, J.P.; Park, H.G. Fire resistant behavior of newly developed bottom-ash-based cementitious coating applied concrete tunnel lining under RABT fire loading. *Constr. Build. Mater.* **2010**, *24*, 1984–1994. [CrossRef]
34. Kim, H.; Jeon, J.; Lee, H. Workability, and mechanical, acoustic and thermal properties of lightweight aggregate concrete with a high volume of entrained air. *Constr. Build. Mater.* **2012**, *29*, 193–200. [CrossRef]
35. Antonio, J.; Mateus, D. Influence of low frequency bands on airborne and impact sound insulation single numbers for typical Portuguese buildings. *Appl. Acoust.* **2015**, *89*, 141–151. [CrossRef]
36. Takao, N.; Xuemei, J.; Isao, M.; Shigeo, S. The influence of the sound absorption ability by the aggregate size and void ratio of porous concrete about sound absorption characteristics of porous concrete. *Proc. Jpn. Constr. Inst.* **2001**, *23*, 163–168.
37. Park, S.B.; Seo, D.S.; Lee, J. Studies on the sound absorption characteristics of porous concrete based on the content of recycled aggregate and target void ratio. *Cem. Concr. Res.* **2005**, *35*, 1846–1854. [CrossRef]
38. Nguyen, L.; Beaucour, A.-L.; Ortola, S.; Noumowé, A. Influence of the volume fraction and the nature of fine lightweight aggregates on the thermal and mechanical properties of structural concrete. *Constr. Build. Mater.* **2014**, *51*, 121–132. [CrossRef]
39. Rossignolo, J.A.; Agnesini, M.V.; Morais, J.A. Properties of high-performance LWAC for precast structures with Brazilian lightweight aggregates. *Cem. Concr. Compos.* **2003**, *25*, 77–82. [CrossRef]
40. The State Planning Organization. *Five Year Development Plan Mining Specialized Commission Report*; Industrial Raw Materials Sub-Commission Chemical Industry Raw Materials Working Group Report; DPT: Ankara, Turkey, 2011; p. 179.
41. Valaskova, M.; Martynková, G.S. *Clay Minerals in Nature: Their Characterization, Modification and Application*; BoD–Books on Demand: Norderstedt, Germany, 2012.
42. Hashem, F.S.; Amin, S.M.; El-Gamal, S.M.A. Chemical activation of vermiculite to produce highly efficient material for Pb2+ and Cd2+ removal. *Appl. Clay Sci.* **2015**, *115*, 189–200. [CrossRef]
43. Morales, S.D.; Rodrigues, E.M.S.; Lamarão, C.N.; Marques, G.T.; Rente, A.F.S. New sodium activated vermiculite process. Testing on Cu2+ removal from tailing dam waters. *J. Hazard. Mater.* **2019**, *366*, 34–38. [CrossRef] [PubMed]
44. Cruz, R.; Dolores, M.; Nieto, J.M. Chemical and structural evolution of "metamorphic vermiculite" in metaclastic rocks of the Betic Cordillera, Málaga, Spain: A synthesis. *Can. Mineral.* **2006**, *44*, 249–265. [CrossRef]
45. Weaver, C.E.; Pollard, L.D. The Chemistry of Clay Minerals. In *Developments in Sedimentology*; Elsevier: New York, NY, USA, 1973; Volume 15, 213 p.
46. Zhang, H.; Zihao, C.; Lu, L. Effect of nanozinc oxide and organic expanded vermiculite compound on antiaging properties of SBR modified bitumen. *J. Mater. Civ. Eng.* **2017**, *29*, 4017204. [CrossRef]
47. Strand, P.R. *Vermiculite, Industrial Minerals and Rocks*; Lefond, S.J., Ed.; Industrial Mineral and Rocks, The Society of Mining Engineers of American Institute of Mining, Metallurgical and Petroleum Engineers, Inc.: New York, NY, USA, 1983; Volume 2, pp. 1375–1381.
48. Yeğinobalı. *Use in Concrete with Silica Fume Cement*; Cement Manufacturers Association of Turkey: Ankara, Turkey, 2007.

49. Değirmenci, A. The Effect of Silica Fume Additive on Reinforced Concrete Steel Corrosion. Master's Thesis, Gazi University Institute of Science and Technology, Ankara, Turkey, 2006.
50. Şimşek, O. *Concrete and Concrete Technology*; Seçkin Publishing: Ankara, Turkey, 2007.
51. Malhotra, V.M. Fly ash, slag, silica fume, and rice husk ash in concrete: A review. *Concr. Int.* **1993**, *15*, 23–28.
52. Subaşı, S.; Beycioğlu, A.; Sancak, E.; Şahin, İ. Rule-based Mamdani type fuzzy logic model for the prediction of compressive strength of silica fume included concrete using non-destructive test results. *Neural Comput. Appl.* **2013**, *22*, 1133–1139. [CrossRef]
53. Qing, Y.; Zhang, Z.; Kong, D.; Chen, R. Influence of nano-SiO2 addition on properties of hardened cement paste as compared with silica fume. *Constr. Build. Mater.* **2007**, *21*, 539–545. [CrossRef]
54. Yildirim, Z.B.; Murat, K.; Volkan, O. Optimisation of Marshall Design criteria with central composite design in asphalt concrete. *Int. J. Pavement Eng.* **2018**, *21*, 666–676. [CrossRef]
55. Miličević, I.; Nina, Š.; Dubravka, B. Optimizing the Concrete Mixture made with Recycled Aggregate Using Experiment Design. In Proceedings of the Recent Advances in Fluid Mechanics and Heat & Mass Transfer, Florence, Italy, 23–25 August 2011; WSEAS Press: Boston, MA, USA, 2011; pp. 110–115.
56. Rooholamini, H.; Hassanim, A.; Aliha, M.R.M. Evaluating the effect of macro-synthetic fibre on the mechanical properties of roller-compacted concrete pavement using response surface methodology. *Constr. Build. Mater.* **2018**, *159*, 517–529. [CrossRef]
57. Gu, B.-W.; Lee, C.-G.; Park, S.-J. Application of response surface methodology and semi-mechanistic model to optimize fluoride removal using crushed concrete in a fixed-bed column. *Environ. Technol.* **2018**, *39*, 616–627. [CrossRef]
58. Adamu, M.; Bashar, S.M.; Shahir, M.L. Mechanical properties and performance of high volume fly ash roller compacted concrete containing crumb rubber and nano silica. *Constr. Build. Mater.* **2018**, *171*, 521–538. [CrossRef]
59. Asadzadeh, S.; Khoshbayan, S. Multi-objective optimization of influential factors on production process of foamed concrete using Box-Behnken approach. *Constr. Build. Mater.* **2018**, *170*, 101–110. [CrossRef]
60. Kockal, N.U.; Ozturan, T. Optimization of properties of fly ash aggregates for high-strength lightweight concrete production. *Mater. Des.* **2011**, *32*, 3586–3593. [CrossRef]
61. Mermerdaş, K.; Algın, Z.; Oleiwi, S.M.; Nassani, D.E. Optimization of lightweight GGBFS and FA geopolymer mortars by response surface method. *Constr. Build. Mater.* **2017**, *139*, 159–171. [CrossRef]
62. Del Coz Diaz, J.J.; Garcia-Nieto, P.J.; Alvarez-Rabanal, F.P.; Alonso-Martínez, M.; Dominguez-Hernandez, J.; Perez-Bella, J.M. The use of response surface methodology to improve the thermal transmittance of lightweight concrete hollow bricks by FEM. *Constr. Build. Mater.* **2014**, *52*, 331–344. [CrossRef]
63. Lee, S.A.; Jung, C.W.; Kim, W.J.; Ahn, J.H. Optimized mixing design of lightweight aerated concrete by response surface analysis. *J. Korea Concr. Inst.* **2009**, *21*, 745–752. [CrossRef]
64. EN 12504-4. *Concrete Tests—Part 4: Determination of Ultrasonic Pulsed Wave Velocity*; Turkish Standards Institution: Ankara, Turkey, 2012.
65. EN 1015-11. *Methods of Test for Mortar for Masonry—Part 11: Determination of Flexural and Compressive Strength of Hardened Mortar*; Turkish Standards Institution: Ankara, Turkey, 2013.
66. Montgomery, D.C. *Design and Analysis of Experiments*, 7th ed.; John Wiley & Sons: New York, NY, USA, 2009.
67. Montgomery, D.C. *Design and Analysis of Experiments*; John Wiley and Sons: New York, NY, USA, 2012; 656p.
68. Mosaberpanah, M.A.; Eren, O. Statistical models for mechanical properties of UHPC using response surface methodology. *Comput. Concr.* **2017**, *19*, 667–675.
69. Mosaberpanah, M.A.; Ozgur, E. Statistical flexural toughness modeling of ultra high performance concrete using response surface method. *Comput. Concr.* **2016**, *17*, 477–488. [CrossRef]
70. Mohammed, B.S.; Yen, L.Y.; Haruna, S.; Huat, M.L.S.; Abdulkadir, I.; Al-Fakih, A.; Liew, M.S.; Zawahi, N.A.W.A. Effect of Elevated Temperature on the compressive strength and durability properties of crumb rubber engineered cementitious composite. *Materials* **2020**, *13*, 31516. [CrossRef]
71. Mohammed, B.S.; Adamu, M. Non-destructive evaluation of nano silica-modified roller-compacted rubbercrete using combined SonReb and response surface methodology. *Road Mater. Pavement Des.* **2019**, *20*, 815–835. [CrossRef]
72. Vahid, V.; Karami, A.; Sheydaei, M. Central composite design optimization of Rhodamine B degradation using TiO2 nanoparticles/UV/PVDF process in continuous submerged membrane photoreactor. *Chem. Eng. Process. Process. Intensif.* **2017**, *116*, 68–75.
73. Harrington, E.C. The desirability function. *Ind. Qual. Control.* **1965**, *21*, 494–498.
74. Derringer, R.S. Simultaneous optimization of several response variables. *J. Qual. Technol.* **1980**, *12*, 214–219. [CrossRef]
75. Kuhn, M. *The Desirability Package*; 2016; The Comprehensive R Archive Network (CRAN); pp. 1–17. Available online: https://cran.r-project.org/web/packages/desirability/vignettes/desirability.pdf (accessed on 1 October 2021).
76. Khan, A.M.; Jamil, M.; Mia, M.; Peminov, D.Y.; Gasiyarov, V.R.; Gupta, M.K.; He, N. Multi-Objective Optimization for Grinding of AISI D2 Steel with AI2O3 Wheel under MQL. *Materials* **2018**, *11*, 2269. [CrossRef]
77. TS EN 12390-5. *Testing Hardened Concrete, Part 5: Flexural Strength of Test Specimens*; Turkish Standards Institution: Ankara, Turkey, 2010.
78. TS EN 12390-3. *Testing Hardened Concrete, Part 3: Compressive Strength of Test Specimens*; Turkish Standards Institution: Ankara, Turkey, 2010.

79. ASTM C 597. *Standard Test Method for Pulse Velocity Through Concrete*; Annual Book of American Society for Testing and Materials: West Conshohocken, PA, USA, 1997.
80. Müzeyyen, B.; Ozbay, E. Optimum design of alkali activated slag concretes for the low oxygen/chloride ion permeability and thermal conductivity. *Compos. Part B Eng.* **2016**, *91*, 243–256.
81. Bulu, P.; Bhattacharjee, B. Performance evaluation of rebar in chloride contaminated concrete by corrosion rate. *Constr. Build. Mater.* **2009**, *23*, 2346–2356.
82. Erdogan, O.; Gesoglu, M.; Guneyisi, E. Transport properties based multi-objective mix proportioning optimization of high performance concretes. *Mater. Struct.* **2011**, *44*, 139–154.